

Residence time of a freshwater embayment connected to a large lake

Francisco J. Rueda¹ and Edwin A. Cowen²

Defrees Hydraulics Laboratory—School of Civil & Environmental Engineering, Cornell University, Ithaca, New York 14853

Abstract

The average length of time water remains within the boundaries of an aquatic system is a key parameter controlling the system's biogeochemical behavior. This timescale, generally referred to as the hydraulic residence time, provides a first-order description of multiple and complex processes that drive transport. The procedures to estimate these transport timescales are reviewed and, through the analysis of numerical simulations, the links between residence timescales and the underlying hydrodynamic processes in a canonical freshwater embayment, Little Sodus Bay (LSB), are explored. LSB has negligible through-flow and is connected permanently to Lake Ontario (LO) through a narrow and shallow channel. Exchange in the channel is the result of a multiple balance where spatial thermal variations (baroclinic forcing), oscillations in water level (barotropic forcing), frictional mixing, wind, and the effects of unsteadiness are all important. The simulations indicate that baroclinic processes are the dominant exchange and mixing mechanisms in embayments like LSB. The largest density gradients across the channel are caused by episodic upwelling events in LO during the stratified season, when exchange rates increase by at least an order of magnitude. The mean residence timescales undergo dramatic variations in time and space and, in general, are comparable to the timescales of the systems' variability itself. The simulations reveal that temporal variations of mean residence timescales occur at interannual, seasonal, and down to synoptic timescales, and are closely related to the occurrence and frequency of upwelling events.

The average length of time water remains within the boundaries of an aquatic system (hydraulic residence time) has been proposed in the literature to explain a range of water quality phenomena such as the variability in lake eutrophication processes, thermal stratification, isotopic composition, alkalinity, dissolved organic carbon concentration, elemental ratios of heavy metals and nutrients, mineralization rates of organic matter, and primary production (*see* Monsen et al. 2002, for a list of references). The experiments of Fussman et al. (2000) go further, suggesting that the hydraulic residence time is a key parameter controlling the structure of aquatic ecosystems and the extent that these systems are self-organized or dominated by exogenous influences. In spite of the biological and chemical implications of the hydraulic residence time, there exist wide spread misconceptions and confusion among aquatic scientists on suitable methods for its determination (e.g., Monsen et al. 2002).

The basic concepts on transport timescales and their application to coastal environments are laid out in the works of Zimmerman (1976) and Dronkers and Zimmerman (1982). There, the most commonly used terms to measure the retention of water or scalar quantities transported in the water are carefully defined, and suitable experiments are presented to calculate the defined timescales, with examples for coastal environments. More recently, Monsen et al. (2002) describe the procedures used to calculate these timescales in idealized systems and show the pitfalls of such procedures when applied to natural systems. These issues are illustrated using depth-averaged numerical simulations in a tidal shallow lake in the Sacramento–San Joaquin River Delta. Although Monsen et al. (2002) raise very interesting issues regarding the influences of (1) unsteady flow; (2) spatial variability of bathymetry, circulation, and transport timescales; and (3) tidal oscillations in the calculation of timescales, their objective is limited to a particular case in a coastal environment that they use to stimulate critical thinking.

The literature on hydraulic residence timescales (e.g., Zimmerman 1976; Dronkers and Zimmerman 1982; Sanford et al. 1992; among others) has focused on environments forced by energetic tidal oscillations, and hence, with relatively short transport timescales. In this work we explore the links between hydrodynamic processes and the transport timescales in Little Sodus Bay (LSB, 43°20'N, 76°42'30''W, Fig. 1), a weakly forced lacustrine system. LSB is a freshwater embayment permanently connected to Lake Ontario (LO) through a shallow (3 m), narrow (75 m), and long (550 m) channel. As shown by Rueda and Cowen (2005), exchange in LSB is forced by variable and weak winds, spatial thermal variations, and oscillations (seiches) in the lake level, which, even in extreme cases, are at most on the order of 10 cm. Through-flow, however, is negligible: the estimated mean daily discharge Q from the contributing water-

¹ Present address: Instituto del Agua, Universidad de Granada, 18071—Granada (Spain).

² Corresponding author (each20@cornell.edu).

Acknowledgments

We thank all the researchers working in the Lake Ontario Biocomplexity Study, and in particular to Gail Steinhart, Andrea Parmeter, and Rebecca Doyle. Thanks to Keith L. Eggleston, Regional Climatologist at the Northeast Regional Climate Center, Cornell University, and Jim Nugent, Chemist from Monroe County Water Authority (4799 Dewey Avenue, Rochester, New York 14612). Their data was helpful in drawing the main conclusions of this research. We are indebted to the reviewers of this manuscript, whose significant time and constructive criticism substantially reshaped and strengthened this manuscript.

Funding was provided by the National Science Foundation (NSF): Biocomplexity in the Environment Program (OCE-0083625) and CTS-0093794, and the Office of Naval Research (ONR) N00014-98-1-0774.

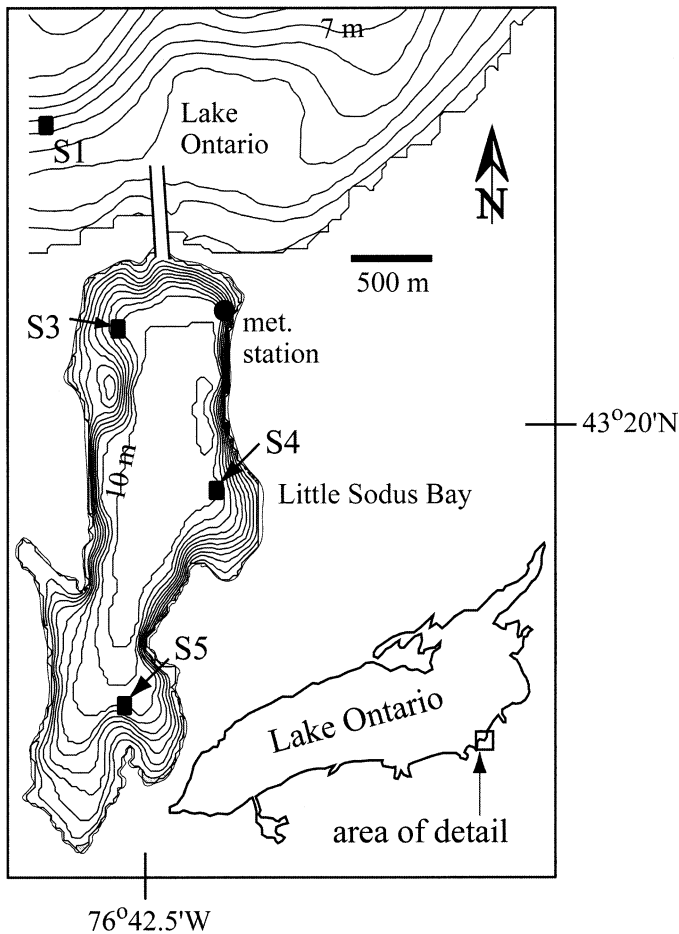


Fig. 1. Location and bathymetric map of LSB. Contours are shown every meter, and the 10-m and 7-m isobaths are shown in LSB and LO, respectively. Thermistor chain locations are shown as black squares and identified as S1, S2, S3, S4, and S5.

shed into the embayment is approximately $0.15 \text{ m}^3 \text{ s}^{-1}$. Dividing the volume of LSB (ca. $2 \times 10^7 \text{ m}^3$) by Q , a widely used approach to estimating residence times in aquatic systems, one gets a timescale of 1,500 d. Although this estimate is flawed (discussed in detail below), it suggests that the mean residence timescales in weakly forced environments are expected to be comparable to the timescales of the systems' variability itself, such as those associated with seasonal changes in stratification. Hence, the analysis of residence times in weakly forced systems needs to be done across seasonal and interannual timescales. Given the inherent spatial and temporal limitations of observational programs and the complexities that result from multiple forcing mechanisms, we approach the problem of determining basin scale circulation, exchange, and hydraulic residence timescales by combining the analysis of field observations (see Rueda and Cowen 2005 for details) with time-resolved unsteady three-dimensional (3-D) numerical simulations.

Background

Transport timescales: Definitions—Any particle entering a lake embayment for the first time at time t_0 and at a lo-

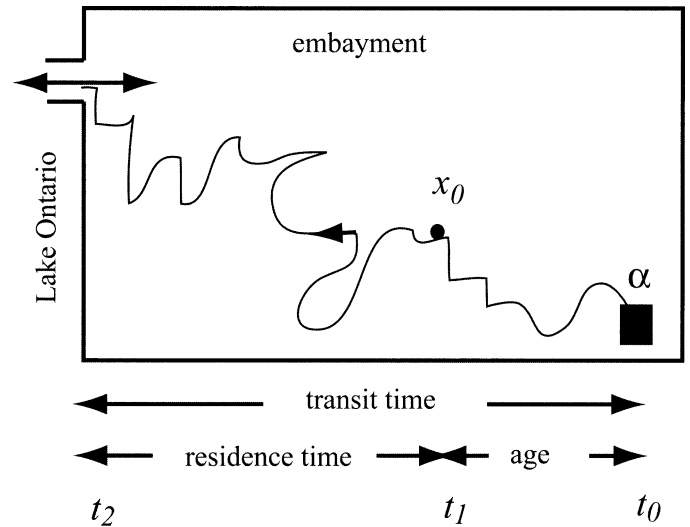


Fig. 2. Definition sketch of transport timescales (transit time, residence time, and age) for an individual particle entering a bay at time t_0 . The entering location, α , represents either a stream or, in semienclosed bays, a birth point of a living organism.

cation α will describe a trajectory $x'(\alpha, t, t_0)$, ultimately leaving the embayment at time t_n . The time interval that a particle requires to cover its path from inlet to outlet (from time t_0 to t_n) is defined to be its *transit time*. The portion of the transit time between the time a particle arrives at a point within the embayment, x_0 (strictly speaking after arriving for the first time at x_0 , since a particle may pass through x_0 more than once), and time t_n is defined to be its *residence time*. The portion of the transit time between time t_0 and the time of first arrival at x_0 is defined as the particle's *age* (see Fig. 2). A second particle released at the same time t_0 and in the close neighborhood of α will most probably describe a completely different trajectory $x''(\alpha, t, t_0)$, due to turbulence and chaotic advection, and will have a different transit time. Given the potential for temporal unsteadiness of the system, along with chaotic advection, a particle's trajectory, and hence its transit time, residence time, and age, are strong functions of t_0 and α . The residence time of an ensemble of particles released at time t_0 and in the close neighborhood of α can be characterized by its probability density function, or pdf. This pdf is termed the residence time distribution, or RTD. The RTD provides a first-order description of transport in the aquatic system, and, as just argued, will depend on α and, in the case of unsteady systems (i.e., all natural systems), t_0 .

A bulk or integrative description (with no spatial dependence) of the transport characteristics of a water body is also definable if instead of tracking an ensemble of particles occupying a limited volume in the neighborhood of a given point α at t_0 , one tracks an ensemble of particles distributed within the entire water body at t_0 . The pdf of the residence time for the ensemble of particles distributed instantaneously throughout the entire basin will be here identified as the flushing time distribution (FTD). In unsteady systems, this FTD is also a function of t_0 .

Characterization of RTD and FTD—To estimate the RTD, conservative tracers are injected, either instantaneously—known as the pulse method—or continuously—known as the step method (Dronkers and Zimmerman 1982; Levenspiel 1999). The pulse method is preferred over the step method, since the latter produces smooth results that tend to hide higher-frequency effects (*see* p. 304 in Levenspiel 1999) and is more appropriate for the analysis of steady-state systems. In the pulse method a mass, m_0 , of tracer is injected at time t_0 and at location α , and the time varying tracer mass, $m(t)$, remaining in the water body is monitored. The quantity $m(t)$ is found from the spatial integration of the measured concentration field within the water body, and its decline over time reflects the net rate at which tracer leaves the water body. If none of the tracer that leaves the system ever returns, the residence time of a tracer particle is the time it takes that particle to leave the water body, and the rate of mass loss as a function of time, $r(t)$, provides the RTD, which we will denote $\varphi(t)$ (Hilton et al. 1998):

$$r(t) = \varphi(t) = -\frac{1}{m_0} \frac{dm}{dt} \quad (1)$$

Equation 1 shows that the RTD has units of $[T]^{-1}$. The *mean residence time*, based on the first moment of $r(t)$, can then be calculated as (e.g., Hilton et al. 1998)

$$\tau_r = \int_0^{\infty} r(t)t \, dt = -\frac{1}{m_0} \int_0^{\infty} \frac{dm}{dt} t \, dt = \frac{1}{m_0} \int_0^{\infty} m(t) \, dt \quad (2)$$

As pointed out by Hilton et al. (1998), “if there is return of tracer from the outlet, or even potentially tracer leaving and returning through the inlet in flow reversing systems, $m(t)$ does not reflect a unique composition of tracer particles and $r(t)$ will not reflect the actual distribution of residence times, $\varphi(t)$. However, the calculation of mean residence time based on $r(t)$ is still valid.”

To estimate the FTD at time t_0 , tracer is initially distributed uniformly throughout the system. The FTD is then calculated as in Eq. 1 and the mean flushing time as in Eq. 2.

Biogeochemical behavior of aquatic systems and the RTD—The behavior of biological–chemical reactors depends critically on the hydraulic residence time of the system. To illustrate this point, consider an elementary, irreversible, first-order reaction of $A \rightarrow B$ in a homogeneous batch (nonflow) reactor. The integrated rate equation yields the amount of A in the system at any time t , and is given by

$$\frac{[A]}{[A]_0} = \exp(-kt) \quad (3)$$

where $[A]_0$ is the initial concentration of species A and k , the reaction rate, has units of $[T]^{-1}$. For a given molecule of A , the probability that it will react during time t (the cumulative distribution function of reaction time) is given by

$$p_r = 1 - \exp(-kt) = 1 - \frac{[A]}{[A]_0} \quad (4)$$

In a single continuous-flow reactor, molecules that have been in the system for a long time will have a high reaction

probability, whereas those that have been in the system for a short time will have a low reaction probability. The probability that any given molecule reacts while it is in the system can be calculated by weighting the simple (batch) reaction probability, derived above, with the RTD, $\varphi(t)$, i.e.,

$$\bar{p}_r = \int_0^{\infty} p_r f(t) \, dt = \int_0^{\infty} [1 - \exp(-kt)] \varphi(t) \, dt \quad (5)$$

where the bar represents the reaction probability in the whole system. Combining Eqs. 4 and 5 one obtains the ratio of the concentration of species A at the outlet to the concentration at the inlet (an index of performance), which takes the form

$$\frac{[A]_{\text{out}}}{[A]_{\text{in}}} = \int_0^{\infty} \exp(-kt) \varphi(t) \, dt \quad (6)$$

Equation 6 shows that to predict the course of any irreversible first-order reaction in a flow system, we only need to know the RTD and the reaction rate constant. It is clear from Eq. 6 that the influence of the physical timescales of transport on the performance of the reactor will depend on the magnitude of the reaction timescale $\tau_{\text{reac}} = 1/k$. A long tail in the RTD will not effect a fast reaction, whereas a slow reaction will be strongly effected by the details of the RTD.

The biogeochemical performance, defined as the ratio of species concentration at the outlet to the concentration at the inlet, only depends on the first moment of the RTD for idealized flow reactors (e.g., Clark 1996). However, to characterize the biogeochemical behavior of more general types of reactors, including environmental systems, one needs to fully determine the shape of the RTD/FTD.

Transport processes and the RTD—The processes involved in the transport of particles from any point in the embayment until they reach the lake are classified here, for the sake of clarity, into “exchange” processes, acting in the channel, and “internal mixing” processes, acting within the embayment. The difference between internal mixing and exchange timescales can be better understood using two idealized flow reactor models: the continuous stirred tank reactor (CSTR) and the plug-flow reactor (PFR, e.g., Levenspiel 1999). In the CSTR internal mixing is considered infinitely fast and the mean residence time is set by the rate at which exchange takes place. At the other extreme, in the PFR the mean residence time is controlled by the rate particles move within the reactor (internal mixing in our semantics), and the exchange processes do not set the RTD. Even though exchange and mixing processes are considered separately, they need to be jointly considered in the examination of basin water residence times since they are inextricably linked in the determination of mass fluxes across the channel (e.g., Ivey 2004). The baroclinic forcing, for example, in the channel is determined by the density in the respective basins, which is influenced by the dynamics within the basins themselves.

Aquatic scientists have focused considerable attention on exchange processes, assuming that water bodies function as CSTRs, with instantaneous internal mixing. Under this assumption, and considering the system to be at steady state, the mean residence time is uniform throughout the basin and

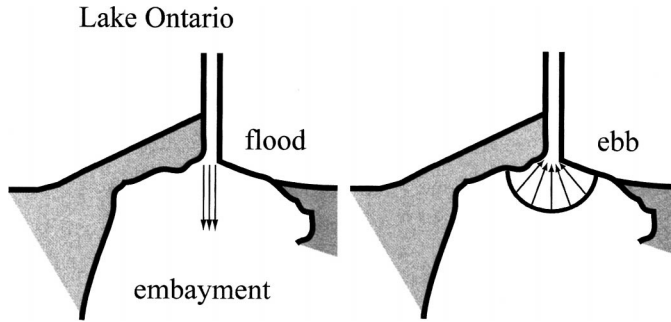


Fig. 3. Stommel and Farmer's (1952) visualization of flood and ebb flows at an inlet, adapted to the geometry of LSB. The flood flow enters as a confined jet, while the ebb flow waters are drawn from all around the mouth in the form of a potential flow to a sink.

is easily calculated as the ratio of the volume of the body, V_0 , to through-flow, Q , i.e.,

$$\tau_r = \frac{V_0}{Q} \quad (7)$$

The mean residence time in this case is identical to the mean flushing time. For tidal systems with negligible through-flow (as in LSB), Eq. 7 can also be applied at intertidal time-scales. Q in tidal systems is calculated as the ratio of the tidal prism (the domain volume between high and low tide marks) and the tidal period. This is the classical "tidal prism" method (Sanford et al. 1992). Although the assumption of instantaneous internal mixing is better in "highly" energetic environments (such as coastal lagoons), it is rarely good, and, in weakly forced systems, such as LSB, it is completely errant. In such "low-energy" environments, as will be demonstrated below, internal mixing processes determine to a large degree the rate at which lake water exchanges with the system, and hence the residence time.

The importance of the internal mixing processes can be better understood if we apply Stommel and Farmer's (1952) visualization of flood and ebb flows to LSB inlet, as shown in Fig. 3. Although the assumption underlying Fig. 3, that water level changes are the dominant mechanism of exchange, is not strictly true, the conclusions remain the same. Figure 3 suggests that the same fluid mass is not transferred in and out of the basin on each tidal (event) cycle, the difference being a net, or residual, mass transfer. The volume of water involved in the exchange, a jet during flood (filling of LSB) or the potential flow region during ebb (draining of LSB), will be, in general, much smaller than the total volume of the embayment. To determine net exchange rates the question that needs to be answered is how rapidly the net water mass introduced during a tidal (event) cycle is mixed with the rest of the embayment water. In other words, at what rate is water at points in the embayment able to reach the area of active exchange? If this rate is low (low internal mixing) a phenomenon known as *short-circuiting* (e.g., Andradóttir and Nepf 2001; Rose et al. 2004) occurs, in which only water from the immediate vicinity of the inlet is involved in the exchange, and the RTD curves show long tails. If the rate at which water at all points in the embayment reaches the active exchange zone is high (strong internal mixing)

then the system approaches the idealized case of the CSTR. The comparison of the exchange rates calculated using a 3-D model with those predicted by the CSTR model becomes a measure of the efficiency of internal mixing.

Materials and methods

The computational model—Numerical simulations of water circulation and exchange in LSB were conducted with a 3-D free surface hydrodynamic model, Si3D (see Smith 1997; Rueda 2001; Rueda and Schladow 2002). Si3D is based on the continuity equation for incompressible fluids, the Reynolds-averaged form of the Navier–Stokes equations for momentum, the transport equation for temperature, and an equation of state relating temperature to fluid density. The governing hydrodynamic equations are solved in layer-averaged form using a semi-implicit, three-level, leapfrog-trapezoidal finite difference scheme on a staggered Cartesian grid. The scalar transport equation is solved using a two-level semi-implicit scheme that uses operator splitting. Only the vertical components of transport are treated implicitly, using the Crank–Nicholson or trapezoidal method for diffusion and the beta method (Gross et al. 1998) for advection; the 1-D advection operators in the horizontal directions are discretized with flux-limiter methods. The corrected fluxes are constructed with the monotone upstream differencing scheme, the Lax–Wendroff second-order method, and the Van Leer MC limiter. Turbulent mixing is represented in the 3-D model following the level 2.5 Mellor–Yamada hierarchy of turbulence closure models (Kantha and Clayson 1994). Horizontal mixing of momentum is parameterized using a Laplacian operator with mixing coefficients determined with a Smagorinsky-type model (e.g., Griffies and Hallberg 2000). To improve the representation of downslope flow processes in the Cartesian geometry, a bottom boundary layer model (BBLM) was applied along the steep slopes of the north end of LSB in the vicinity of the channel. The BBLM is similar to that of Beckmann and Doscher (1997), with the only difference being that three cells form the bottom boundary layer. This ad hoc procedure proved to be effective in representing correctly the distribution of water masses within LSB as revealed by the temperature observations collected during a 48-d period starting on day 200, 2002 (see following).

The computations were conducted on a domain that includes a small portion of LO using $75 \times 75 \times 0.5$ -m grid cells (the computational domain is the same as shown in Fig. 1). A small portion of the lake was included so as to provide a reasonable representation of the temperature adjustment between the channel water and the lake water, and hence of the exchange processes through the channel. Assuming that Stommel and Farmer's (1952) visualization of tidal exchanges (Fig. 3) provides a first-order representation of the exchange processes when applied to the LSB-LO system, one can estimate the area from which water will be drawn during a flood event into the embayment from a velocity and a timescale, and geometric characteristics of the connection. Using values of $U_0 = 1 \text{ m s}^{-1}$, the maximum velocity expected in the channel, corresponding to an amplitude of wa-

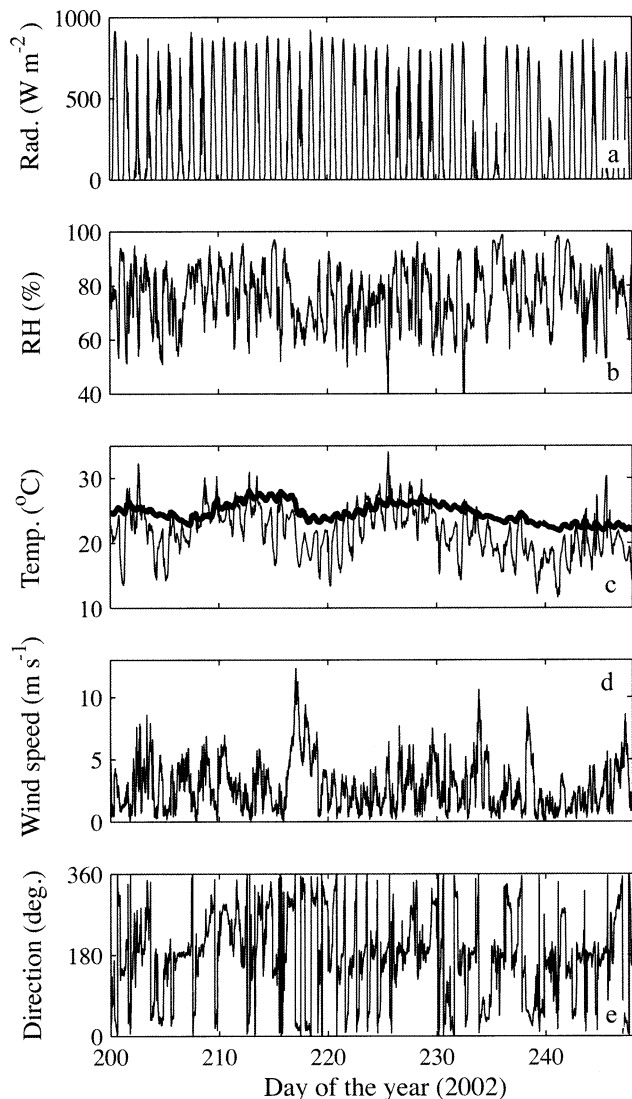


Fig. 4. Time series of meteorological variables collected in LSB from day 200 to day 248, 2002. (a) Solar radiation; (b) relative humidity; (c) air (thin line) and surface water (thick line)—temperatures; (d) wind speed; and (e) wind direction.

ter level oscillations of about 10–15 cm in a typical period of $T = 1$ h (see Rueda and Cowen 2005), the area draining into the channel during flood can have a radius of about 250 m. By using a region that extends to approximately 250 m in each coordinate direction we are able to represent the exchange with LO driven by water level oscillations at reasonable computational cost.

The discretization parameters were selected on the basis of practicality and stability considerations. The spatial resolution was dictated by the need to adequately represent, to first order, the physics in the narrow (~ 75 m) and shallow (~ 3 m) connection between the embayment and the lake. With this level of spatial resolution, the time step, Δt , was set to 60 s to comply with the Courant-Friedrich-Lévy (CFL) condition ($U\Delta t\Delta x^{-1} < 1$, U being the velocity scale) that guarantees numerical stability. The velocities in the channel, depending on the magnitude of water level oscillations, can

Table 1. Depths of thermistors in stations S1, S3, and S4 at the time of deployment.

Station	Depths of thermistors (m below surface)
S1	0.5, 1.5, 3.5, 5.0, 6.5
S3	0.5, 2.5, 4.5, 6.5, 8
S4	0.5, 2, 3.5, 5.0, 6.5, 8.5, 10.5

be as high as $50\text{--}60$ cm s^{-1} . The Courant number ($U\Delta t\Delta x^{-1}$) is close to 1, which gives a sense of the restrictions that the need to represent exchange processes across small channels imposes on the numerical algorithms.

The observational data set—To ensure that the model provides a valid representation of the circulation and exchange processes taking place in LSB, a 48-d period, starting on day 200, 2002, was simulated with the model. The simulated time series of temperature profiles at two points (S3 and S4 in Fig. 1) were compared with the temperature observations collected at those same points and during that same period (see validation results). The model was initialized with a temperature profile constructed by averaging the thermistor records for day 200 and then interpolating linearly from the depth of the thermistors to the vertical location of the center of each computational cell. All isotherms were flat at the beginning of simulations. The model was forced using observed temperatures in LO (S1 in Fig. 1), heat and momentum heat fluxes estimated from local meteorological variables, and observed water level changes in LSB (measured at S2, Fig. 1). Figure 4 shows the time series of local atmospheric variables recorded on 15-min intervals at the meteorological station shown in Fig. 1. Solar radiation, wind speed, and direction were measured approximately 5 m above lake level. All other meteorological sensors were located 3 m above the water surface. The temperature records exhibit change both at diurnal and synoptical timescales. Three troughs can be distinguished in the temperature time series, around days 205, 220, and 240. Most of the time surface water temperature in LSB was above air temperature, and consequently the atmospheric boundary layer about the air–water interface was generally unstable. The embayment was subject most frequently to relatively weak northerly and, in particular, southerly winds, most probably of local nature (lake breezes). The strongest wind events affecting LSB were from the west–northwest (synoptic). The maximum wind speed recorded in LSB during the study period was 13.3 m s^{-1} on day 234 from the north. Heat and momentum fluxes were estimated from local meteorological variables using the bulk-parameter method of Fairall et al. (1996). These estimates, which take into account the effects of atmospheric stability on the air–water heat and momentum transfer, were provided to the numerical model as surface boundary conditions.

Thermistor chains, equipped with Seabird SBE39 temperature loggers, were deployed at three different locations in LSB and LO (stations S1, S3, and S4 in Fig. 1) to monitor the evolution of water temperature at different depths. Table 1 shows the vertical position of the thermistors in each string at the time of deployment (on day 193, 2002). In all cases,

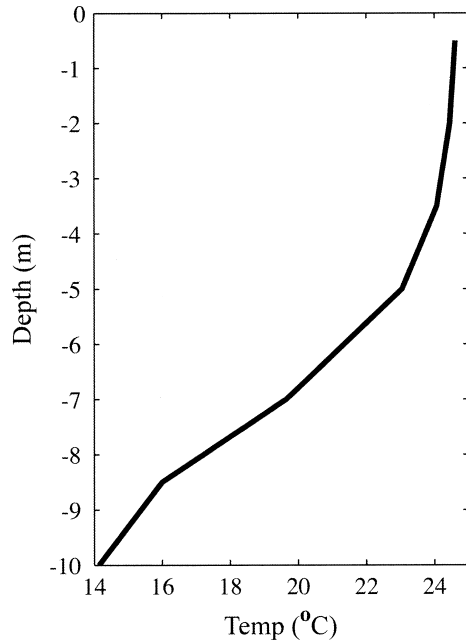


Fig. 5. Average temperature profile at station S4 during the 48-d period of study.

the thermistors were programmed to record water temperatures at 2-min intervals. The shallowest thermistor was attached to a surface buoy. All others were attached to a line connecting a subsurface buoy to a 50-kg (in air) weight on the bottom. Hence, the vertical position of all thermistors below 0.5 m is fixed and does not change with the water level. Figure 5 shows the average temperature profile for the 48-d period at S4, obtained by averaging the 1-min temperature records. The profile shows a 4-m surface mixed layer, with temperature changes of less than 1°C, and a thick metalimnion with temperature gradients of ca. 1.7°C m⁻¹.

Figure 6 shows the time series of lake level and water temperature provided to the model as boundary conditions in LO. Water level changes in LO were estimated from 2-min pressure records collected at station S5 within LSB (Fig. 1). All attempts to make pressure measurements in LO were unsuccessful. The underwater pressure records were first corrected for atmospheric pressure P_a , using 1-h measurements taken at the meteorological station. The time series was then filtered, using a low-pass seventh-order Butterworth filter, to eliminate signal below 1-h period. The high-frequency signals correspond to seiche motions within LSB. Lake levels, as shown in Fig. 6, undergo oscillations on a wide range of timescales, including seasonal, synoptic (caused by weather phenomena, specifically wind), and sub-diurnal. Oscillations with periods shorter than diurnal include the semidiurnal tides and LO seiches (Rueda and Cowen 2005). Water temperature boundary conditions were constructed by averaging the records from the three shallowest thermistors in S1, located above the bottom of the LSB channel. LO surface temperatures were always lower than LSB surface temperatures (compare Figs. 6 and 5). Episodic winds with strong alongshore (easterly) component or offshore (southerly) component acting during the stratified sea-

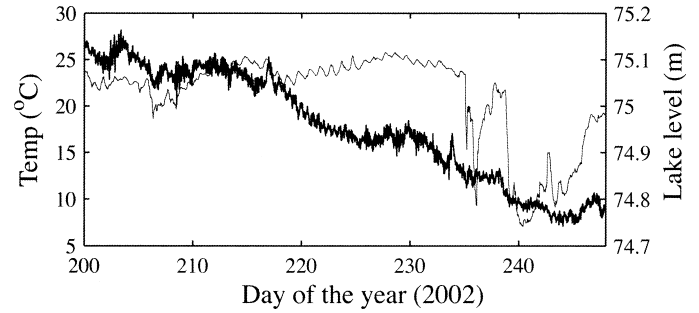


Fig. 6. Boundary conditions used for LO in the numerical simulations. Lake water temperature is shown with a thin line. The evolution of lake levels is shown as a thick line.

son, either on a motionless basin or in phase with basin-scale Kelvin internal waves, can induce upwelling of hypolimnetic water along the south shore of LO, causing the temperature gradients across the channel to increase dramatically. As shown by Rueda and Cowen (2005), the three dips in the LO temperature records correspond to a sequence of upwelling-favorable northeasterly wind events on days 235, 240, and 244. Temperature differences across the channel on these days reached 16°C, which agrees with a typical summer temperature difference between the epilimnetic and hypolimnetic waters in LO (Schwab 1977).

Secchi depth measurements in LSB were taken on a weekly basis at a station close to S4, and their values ranged from 1.2 m on day 218 to 3.4 m on day 224 (see Table 2). Light extinction coefficients η were estimated from Secchi depth readings d following Martin and McCutcheon (1999):

$$\eta = 1.7/d \quad (8)$$

The light extinction coefficient is used in the model to calculate the vertical distribution of shortwave solar radiation in the water column. A 15-min time series of η was constructed by linearly interpolating the values shown in Table 2. It was assumed, for interpolation purposes, that those values were taken at noon on the days shown in Table 2.

Short-term tracer simulations—The simulated 3-D velocity field in LSB for days 200 to 248, 2002 was used to conduct a sequence of tracer release experiments, aimed at evaluating the role played by baroclinic and barotropic processes in replacing the embayment water by lake water. Each of these experiments are 4 d in duration, and are conducted

Table 2. Secchi depth measurements taken during the study period (Doyle and Hairston pers. comm.).

Day (2002)	Secchi depth (m)
197	2.7
203	2.0
210	2.0
218	1.2
224	3.4
231	3.4
239	2.6
245	3.0

every 4 d starting on day 204 and finishing on day 244. A uniform concentration of 100 arbitrary units of tracer is released in the lake and the northern half of the channel. The embayment and the southern half of the channel have initially zero tracer concentration. These two domains, having 0 and 100 units of tracer, are separate by one cell at the center of the channel. Each of these experiments is similar to that proposed by Zimmerman (1976) to characterize the flushing time of a given water body. To determine the flushing time one needs to conduct a long-term simulation until the mass in the embayment reaches a given fraction of its initial concentration. Here, the tracer is only followed as it enters the embayment during 4 d. The reason for doing a succession of short experiments, rather than a unique release at the beginning of the 48-d simulation, is that the mass flux in/out of the embayment is not constant along the 48-d simulation, even if we consider the volumetric flux constant in the channel and assume perfectly mixed conditions. In fact, under such conditions the embayment would behave as a CSTR, and the mass flux into the embayment would decrease exponentially. By using a series of short release experiments, the initial exchange rate and its evolution are characterized, and the conditions that control the exchange and mixing processes are revealed.

Long-term numerical simulations—To examine the spatio-temporal changes in transport timescales, long-term numerical simulations of up to 9 months were conducted. In these simulations, the model was forced with hourly atmospheric records (wind speed and direction, atmospheric pressure, air temperature, relative humidity, solar radiation and cloud cover) generated with the Northeast Regional Climate Center model (DeGaetano et al. 1993, 1994) for Rochester, New York. To drive the model at the LO boundary we used hourly historical records of lake levels at Rochester, New York from the Center for Operational Oceanographic Products and Services (CO-OPS) National Water Level Observation Network databases, and daily water temperatures collected at Shoremont intake (800 m offshore at 8–10 m below the surface, also near Rochester, New York—the authorities are not allowed to reveal its exact location) and provided by the Monroe County Water Authority. Using the velocity field generated in the long-term model runs, tracer release experiments of the type described in the background section were simulated to obtain RTDs and FTDs and their first moments. The simulated RTDs and FTDs were used to examine the linkages between hydrodynamic processes and the transport timescales.

Results and discussion

Validation—As stated in Dee (1995), “model validation involves a broad range of activities: theoretical analysis of model assumptions, numerical analysis of discretization techniques, computational experiments on hypothetical test cases, comparison between model results and laboratory measurements, case studies involving field applications. . . .” Those steps were carefully followed in the selection, formulation, and testing of the Si3D (Rueda 2001; Rueda and

Table 3. Error norms of the three-dimensional temperature simulations (see definitions of error norms in Rueda and Schladow 2003).

	RMSE	ℓ_1	ℓ_2
S3, 0.5 m	0.492	0.0154	0.0201
S3, 2.5 m	0.416	0.0132	0.0171
S3, 4.5 m	0.567	0.0186	0.0241
S3, 6.5 m	1.154	0.0579	0.0760
S4, 0.5 m	0.511	0.0163	0.0207
S4, 2.0 m	0.520	0.0167	0.0212
S4, 3.5 m	0.500	0.0163	0.0207
S4, 5.0 m	0.687	0.0230	0.0295
S4, 7.0 m	0.712	0.0286	0.0349
S4, 8.5 m	0.775	0.0382	0.0468

Schladow 2002). Here only the last step of Dee’s methodology is considered.

Temperature data collected at stations S3 and S4 (Fig. 1) were used for model validation. Only results from the last 40 d of simulation were used in this validation exercise. The agreement between observed and simulated time series of water temperature at the location of the thermistors was quantified using the ℓ_1 , ℓ_2 error norms and the root-mean-square error (RMSE) (see Rueda and Schladow 2002). Table 3 shows these error measures that result from comparing observed and simulated records during the period of validation. Prior to the comparison, and given that we are mainly interested in the long-term evolution of the system, we averaged the records using 3-h bins. The agreement is good and consistent with or better than other 3-D modeling studies of similar water bodies (e.g., Hodges et al. 2000; Jin et al. 2000; Rueda and Schladow 2003). The maximum RMSE encountered in the comparison was 1.1 at 6.5 m below the free surface in S3, a depth where temperature is subject to large oscillations due to internal waves. At all other locations, the RMSE was below 0.8 and the minimum value encountered was 0.41, 2.5 m below the free surface in S3.

Figure 7 shows simulated and observed daily averaged temperature profiles every 4 d during the period of study. It shows that the long-term evolution of stratification in the water column is well-captured by the model: surface temperature, thickness of the surface layer, and the temperature gradient in the metalimnion. By correctly representing the evolution of the thermal structure in the water column (indicative of an appropriate parameterization of wind-driven mixing processes), the model is able to capture the competition between the overturning wind forcing and the stabilizing effect of stratification. The larger magnitude of the error norms found below the surface layer (4–5 m) is probably the result of the large short-term temperature oscillations, induced by internal waves in the metalimnion of the system. Those oscillations are larger at S3, and consequently the error found at S3, 6.5 m, is larger. As shown by Rueda et al. (2003), among others, the phase of the internal waves are rarely captured correctly by 3-D models; simulated and observed phases agree especially after strong wind events when the energy introduced through surface shear is enough to obliterate the internal wave field existing before the event. It is precisely during such events that the metalimnion is

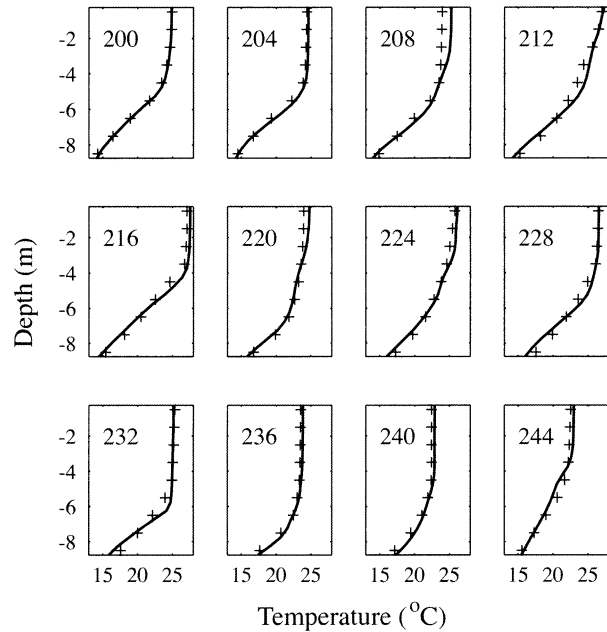


Fig. 7. Simulated (continuous line) and experimental (crosses) daily averaged profiles at S4. Profiles are shown every 4 d (the day of the year is shown in the upper left-hand corner). The experimental values are obtained by linearly interpolating the observed values collected by the thermistors at a 1-m spacing.

able to reach the surface and significant changes in baroclinic forcing may occur. Figure 8 compares simulated and observed time series of isotherm displacements at S3. It shows that, under the influence of strong northerly winds (around day 217), the 23°C isotherm repeatedly reaches the free surface, both in the simulations and observations. The simulated surface temperatures agree within 0.5°C (see Table 3) with the observed values at the northern end of LSB. It is the difference in temperature between the lake and the embayment above the bottom of the channel (i.e., in the first 3 m below the free surface) that controls the magnitude of the baroclinic forcing (e.g., Rueda and Cowen 2005). Hence, by correctly representing the surface temperatures, and its variations, in the vicinity of the lake–embayment connection (Fig. 8), we expect that the model will provide accurate estimates of the magnitude of the baroclinic forcing across the channel and the residual transport.

Both observations and simulations show deep intrusions of cold lake water during the upwelling events after day 240. The temperature, depth, and thickness of such intrusions in the simulated results are reasonably close to the observations. For example, at station S3 on day 244 the 21°C isotherm is at ca. 5 m and 4.9 m from the free surface in the observed and simulated results, respectively; the temperature 7 m below the free surface on that same day is approximately 17.5°C in the observations and 17.9°C in the simulations.

The model results are close to the observations and deemed good. The mismatches can be attributed to a wide range of causes, from observation error in the driving boundary conditions (wind and heat flux, for example, are considered to be uniform, or the Secchi depth measurements were

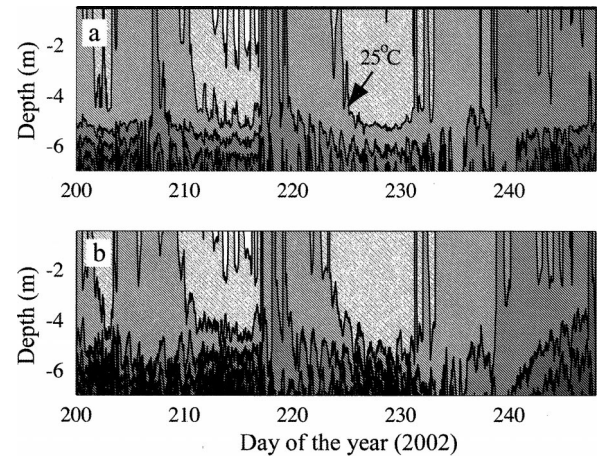


Fig. 8. Isotherm displacements at S3: (a) observed and (b) simulated. Isotherms are shown every 2°C. The 25°C isotherm is marked in (a).

taken on a weekly basis with strong variations) to model errors (e.g., the vertical mixing model or the representation of the varying bathymetry). The model is, though, able to capture the relevant physics to meet the objectives of this study and was used as a tool to investigate the physics and long-term evolution of the exchange of water between LO and LSB.

Mechanisms of exchange and mixing: Role of upwelling events—The results of the short-term tracer release experiments are summarized in Fig. 9. Figure 9a shows the time series of g' , the reduced gravity characterizing surface temperature differences ΔT_c between a point located along the boundary in LO and another located in LSB at station S3, i.e.,

$$g' = g \frac{\rho(T_{LO}) - \rho(T_{S3})}{\rho(T_{LO})} \quad (9)$$

Here g is the acceleration of gravity, $\rho(T_{LO})$ is the density of water in LO determined from its surface temperature, T_{LO} , and $\rho(T_{S3})$ is the density of water in LSB determined from the surface temperature at S_3 , T_{S3} . The value of g' together with the amplitude of the barotropic velocity oscillations U_0 in the channel were shown in Rueda and Cowen (2005) to explain the character of lake–embayment exchange processes. Exchange processes are controlled by barotropic forces under conditions of large U_0 and low g' (i.e., large Froude number defined as the ratio $U_0^2/g'h$). For large values of g' baroclinic processes become the dominant exchange mechanism. Barotropic velocity oscillations in LSB channel are driven by a wide range of forcing phenomena (semidiurnal tides and lake seiches), each with different energy levels and periodicity (see Rueda and Cowen 2005). Hence, U_0 changes from one oscillation to the next. To characterize the evolution of U_0 over the 48-d period we used a statistical descriptor, U_c . For each day j ($j = 1$ through 48), the time series of depth-averaged velocity at the center of the channel $U_j(t)$ was calculated. The value of U_c for day j was calculated as the standard deviation of $U_j(t)$, after detrending.

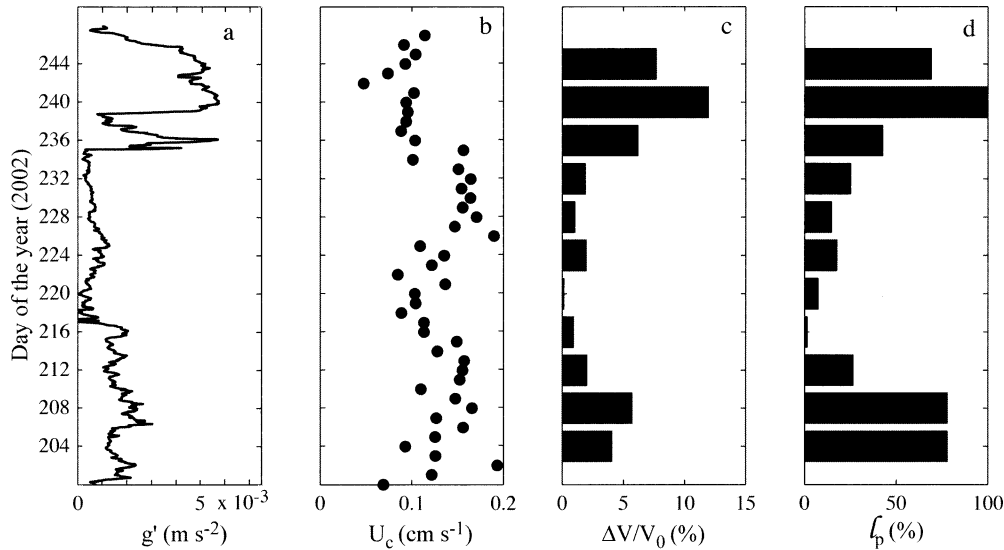


Fig. 9. Results of simulated tracer experiments for summer 2002. (a) Time series of reduced gravity and lake levels. (b) Standard deviation of along-channel depth-averaged velocity fluctuations in a 1-d window. (c) Volumetric exchange rate for the 11 tracer experiments, given in nondimensional form and as a percentage of the initial embayment volume. (d) Penetration length for the 11 tracer experiments (*see* definition in the text).

Figure 9b shows the evolution of U_c for the study period. The volumetric exchange rate ΔV is obtained by dividing the change in tracer mass within the embayment during the 4-d period by the initial concentration C_0 ($=100$ units). This value is given in nondimensional form (Fig. 9c), as a percentage of the volume of water in the embayment at the start of the simulation V_0 . The penetration length l_p shown in Fig. 9d was used, for comparative purposes, as a measure of the internal mixing of lake water within the embayment. To calculate l_p , the 3-D tracer field at the end of each 4-d simulation period was used to calculate a series of cross-sectional average concentrations C_i along the north–south axis of the embayment, i.e.,

$$C_i(i) = \sum_{j=1}^{jm} \sum_{k=1}^{km} C(i, j, k) \times \delta V(i, j, k) \sum_{j=1}^{jm} \sum_{k=1}^{km} \delta V(i, j, k) \quad (10)$$

Here $\delta V(i, j, k)$ is the volume of water within a given computational cell and $C(i, j, k)$ is the concentration of tracer within it. The penetration length l_p was then calculated as the distance from the north end of the embayment to the point where $C_i(i)$ is at least 10% of the concentration in LO (i.e., 10 units), and nondimensionalized using the maximum length of the LSB (3,400 m). Although it is simple and does not allow one to examine 3-D or large-scale horizontal structures in the tracer field, this measure allows us to compare the extent to which lake water is able to penetrate within the embayment under different forcing scenarios. Under strong mixing, lake water could reach the southern end of the embayment at the end of the 4-d simulation and l_p would be then close to 1. If lake and embayment water mix only in the close vicinity of the LSB-LO connection (i.e., short cir-

cuting or weak mixing), l_p would be close to zero. It would be exactly zero if no lake water had entered the embayment in the 4-d simulation period.

Exchange rates calculated from the day-240 release, with $g' = 6 \times 10^{-3} \text{ m s}^{-2}$ ($\Delta T_c \sim 16^\circ\text{C}$) and during the LO upwelling events, were two orders of magnitude larger than the rates for the day-216 release and one order of magnitude larger than the rates for the day-228 release. Almost 12% of the LSB volume entered the embayment in the 4-d simulation starting on day 240, a rate that, if maintained, would have renewed the embayment within 30 d. From days 216 to 220, $g' < 5 \times 10^{-4} \text{ m s}^{-2}$, U_c is low, and only 0.1% of the embayment volume is exchanged. During the tracer experiment of day 228, g' is also small but U_c is larger (the standard deviation of the velocity oscillations is twice that observed on day 216 or 240). The volume of water exchanged is 1% of the embayment volume. The numerical simulations, hence, show that major exchange events coincide with large temperature differences across the lake–embayment connection, which are driven by LO upwelling events.

The penetration length l_p follows a similar pattern, with larger values for larger temperature gradients, which suggests that baroclinic processes are an effective mechanism for internal mixing. Wind, on the other hand, is not as effective at driving internal mixing of lake and embayment water. Wind speeds after day 240 were approximately three times smaller than those observed during days 216 to 220 ($<5 \text{ m s}^{-1}$). The value of l_p under strong winds, however, is almost 10% the value of l_p found for days 240 and on. During the upwelling event of day 240 the internal dynamics of the embayment change dramatically and the whole basin is actively involved in the exchange process. During upwelling events gravitational forces (density differences) bring cold

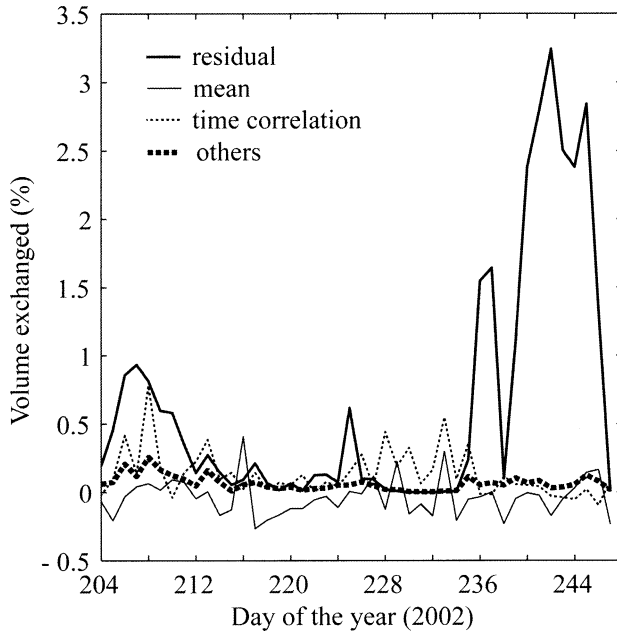


Fig. 10. The 12-h transport volume into LSB in 4-d experiments due to mean advection, time-correlation of cross-sectional averages, residual bidirectional exchange, and other mechanisms. Positive values are into the bay. The 12-h transport volume is normalized by LSB volume and reported as a percentage of this volume.

LO water into the interior of LSB; lake water advances as gravity currents and reaches the end of the embayment within hours (<1 d) after penetration (*see Rueda and Cowen 2005, and also Fig. 8*). The barotropic processes are not as effective at driving exchange: the excursion of an individual particle during a typical 2-h seiche cycle is less than 500 m (recall this is the lake–embayment channel length scale), and considerably smaller than the length of the basin (4 km). Lake water introduced in LSB by barotropic forcing will remain in the northern end of LSB, and will be carried to its southern end by other mechanisms (e.g., wind-driven circulation), which, as shown in Fig. 9d, are inefficient in comparison with gravity-driven currents.

Using simulated velocity and concentration time series at the center of the channel, and following Fischer et al. (1979, p. 255), the transport was decomposed into: (1) mean advection, (2) time-correlation of cross-sectional averages, (3) residual bidirectional exchange or residual circulation, and (4) a residual that accounts for the effects of oscillatory shear flow and any other random motions. The averaging period used for the analysis is 12 h. At this timescale, only the net effects of semidiurnal tides and seiche-induced lake-level oscillations on transport are captured. Term 2 represents the contribution of barotropic processes to transport through the mechanism of exchange illustrated in Fig. 3. Its magnitude will critically depend on mixing rates on either end of the channel. By including part of LO in the simulations of LSB we presume that these mixing rates are reasonably well represented. The contribution of density- and wind-driven processes is contained in the residual circulation transport. Figure 10 shows the daily evolution of the four transport components during the 48 d of simulation.

On average, the residual circulation is the dominant transport process. The relative contribution of the different terms depends, however, on the magnitude of the longitudinal velocity oscillations and the temperature gradients across the channel. During the 4 d after day 220 (low ΔT_c and U_c), both terms 2 and 3 contribute equally to the flow into LSB, working against the mean advection (term 1) that pumps water out of the embayment during a period characterized by a continuous and steady decrease of LO water level (*see Fig. 6*). For the experiment of day 228 (low ΔT_c and large U_c), term 2 is primarily responsible for the exchange, whereas for the day-240 experiment baroclinic transport is by far the dominant process.

Exchange rates: Theoretical models and simulation results—Given that residual circulation is the major contributor to the exchange of water masses through the channel, it is natural to ask what drives this process and whether it is possible to estimate the exchange rates on the basis of simplified models. Most of the literature (mainly in physical oceanography) has assumed that bidirectional exchange through topographic constrictions (either over a sill or through a contraction) is density driven. It is further presumed that plan view changes in channel geometry are smooth and gradual (hence, the problem can be studied in a vertical plane) and that bathymetric variations are also smooth and gradual. Two different analytical models have been proposed to predict the flux under these conditions: (1) the internal hydraulic (IH) model (e.g., Armi and Farmer 1986; Farmer and Armi 1986) and (2) the viscous advective diffusion (VAD) model (e.g., Officer 1976). In the IH model, the maximal volumetric exchange rate through a contraction is

$$Q_{H,c} = \frac{1}{4} B g'^{1/2} H^{3/2} \quad (11)$$

Here B and H are the width and the depth of the channel at the contraction, respectively. Maximal exchange requires that two controls exist, where the internal Froude number is critical, and the hydraulic conditions in the channel are independent of the reservoir conditions on either side (i.e., supercritical flow must occur on the channel-end sides of the controls).

In the VAD model, the volumetric exchange rate through the channel can be calculated as (Hogg et al. 2001)

$$Q_v = \frac{5}{384} \frac{g' H^4}{K_v L} B \quad (12)$$

where L is the length of the channel and K_v is the vertical turbulent eddy viscosity. The exchange rate in the VAD model depends linearly on g' (and roughly linearly on ΔT_c), whereas in the hydraulic model it depends on the square root of g' (and roughly on the square root of ΔT_c).

Hogg et al. (2001) have formulated a conceptual framework that allows one to analyze problems that fall in between the two limiting cases of the IH and VAD model solutions. In their finite thickness interface (FI) model, a three-way balance between viscosity, inertia, and buoyancy determines the exchange rate through a contraction. The ex-

change rate through a smooth flat-bottom contraction, non-dimensionalized by the IH prediction (Eq. 11), is shown in Hogg et al. (2001) to be

$$q_F = 1 - \frac{\alpha(Gr_T A^2)^{-1/4}}{2} \quad (13)$$

where α is a coefficient that Hogg et al. (2001) set to 3.4, $Gr_T = g'H^3/K_v$ is the Grasshof number, and $A = H/L$. To calculate mass fluxes of a given tracer from the volumetric exchange rates using the IH model one only needs to multiply $Q_{H,c}$ (maximal flow through a contraction) by the tracer concentration of LO. In the VAD model it is necessary to solve an equation for tracer concentration in the channel that balances horizontal advection and vertical turbulent diffusion. Once the expression of tracer concentration is found, the tracer mass flux can be calculated as the sum of the fluxes inducing horizontal diffusion and advection, i.e.,

$$M_v = \left[BH \int_0^1 \left(\frac{\partial C}{\partial x} K_H + Cu \right) dz \right] \quad (14)$$

Nondimensionalized by the hydraulic prediction, the mass flux in the VAD model is

$$m_v = \frac{4A^2}{(Gr_T A^2)^{1/2}} + \frac{31(Gr_T A^2)^{3/2}}{362,880} \quad (15)$$

where it has been assumed that the Prandtl number is one. The nondimensional mass flux across a contraction predicted by the FI model is given by

$$m_F = 1 - \frac{2\alpha(Gr_T A^2)^{-1/4}}{3}, \quad \alpha = 3.4 \quad (16)$$

The net transport of mass into LSB, calculated from all the 3-D tracer experiments on a diurnal basis, is plotted in Fig. 11 as a function of the temperature difference across the channel. The 3-D results will be considered here as “observations.” The “predicted” mass fluxes will be those calculated using the IH, VAD, and FI models, and they are also shown on the same plot.

None of the theoretical models provides a satisfactory representation of the “observed” results in all cases. This is, in part, explained by the changing nature of the exchange processes in the LSB-LO channel, as shown in Rueda and Cowen (2005). Rueda and Cowen (2005) show that F_i , the internal Froude number defined as $u_i/(g'h_i)$ where i is the layer number, could be either greater or less than 1, depending not only on ΔT_c but also on the strength of water surface oscillations and wind, which cause increases in the rate of mixing in the water column. For high ΔT_c , the “observations” get closer to the maximal hydraulic prediction, but the IH model (Eq. 11) overpredicts, in most cases, the “observed” fluxes, suggesting that reservoir conditions indeed do influence the exchange flow across the channel (i.e., the fluxes across the channel are submaximal). For weak along-channel temperature gradients the scatter in the data is noticeable, which again suggests that (1) the conditions both in the lake and the embayment need to be considered, or (2) residual flow in the channel is not driven solely by temperature differences.

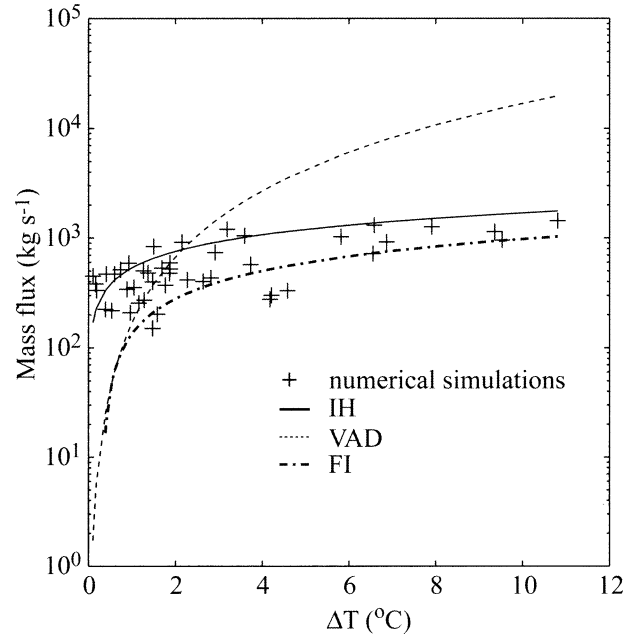


Fig. 11. Mass flux through the lake–bay connection (kg s^{-1}) as a function of along-channel temperature difference. The numerical results represent the average residual component of transport during 12-h intervals. Also plotted are the predictions based on the IH, the VAD, and the FI models. For the VAD model, the average eddy viscosity during 12-h periods is used for the predictions.

In fact, wind can also force the residual circulation in the channel. A simple scaling analysis indicates that the relative magnitude of the wind and the baroclinic forcing in generating residual circulation can be expressed with a Wedderburn number-type parameter:

$$We_g = \frac{h(g'h)}{L(u_*^2)} \quad (17)$$

For $We_g \gg 1$ baroclinic forcing dominates, whereas if $We_g \ll 1$ wind forcing is dominant. Some authors (e.g., Andradottir and Nepf 2001) have used a transition We_g of approximately 9. This criterion is based on the value of We_g at which the surface velocity induced by a horizontal density gradient is cancelled by the wind stress (see eq. 4.106 in Officer 1976). For weak density gradients ($g' \sim 3 \times 10^{-3} \text{ m s}^{-2}$), baroclinic forcing will only dominate wind-driven motions under calm conditions (low winds of up to $\sim 2 \text{ m s}^{-1}$). A careful analysis of mass fluxes and their relation to the N-S component of wind and ΔT_c reveals that for low values of ΔT_c (always colder in LO) minimum mass flux into the embayment occurs under strong northerly winds, increasing as the northerly component diminishes and the wind blows from the south. For low southerly winds, ΔT_c varies from almost 0°C to nearly 16°C .

Transport timescale estimates: Long-term simulations—The results presented in the two previous sections suggest that (1) not all the volume of the embayment is directly involved in the exchange process, and (2) the lake–embayment exchange rate varies with time and is not easily pre-

dicted by theoretical models, which neglect forcing mechanisms (wind stress or bottom friction) that are actively involved in the exchange or presume maximal exchange conditions. Therefore, the ratio $V_0:Q$ is not a good estimate of the mean flushing time and does not provide a valid first-order integral description of the transport in LSB or any other similar embayments. In this section mean residence and flushing timescales are estimated through the simulation of long-term tracer experiments (pulse method), by first building a flux versus time curve and then calculating its first moment (*see Background*). The fluxes are calculated by tracking the total amount of tracer remaining in LSB as a function of time. These numerical experiments are used to explore the spatial and temporal variations of the transport timescales. The choice of lake-level boundary conditions, taken from Rochester, for these experiments is deemed unimportant given that, as shown in the previous sections, the contribution of barotropic processes to the determination of lake–embayment exchange is minor in comparison with density-driven phenomena. The data from Rochester were selected to provide the simulations with a coherent data set, with wind and water level values that were from the same site along the southern coast of LO.

Flushing timescales.—The occurrence of upwelling events along the south shore of LO is episodic, but not uncommon. A visual inspection of the 18-yr daily time series of lake water temperatures used to drive this section's simulations (not shown) reveals a considerable interannual variability in the number and duration of upwelling events and the temperature changes induced by them. This fact, together with the large exchange and mixing rates associated with individual upwelling events observed in the simulations, suggests that there must be interannual changes in the mean flushing timescales of LSB with more active transport rates during years with more or stronger upwelling events. To test this hypothesis several flushing numerical experiments (*see Background section—Characterization of RTD and FTD*) were conducted for the years 1995 and 1999. According to Eq. 11, the duration of an upwelling event Δt_u multiplied by the square root of the mean induced temperature changes ΔT_c provides an appropriate scale of the volume of water V_u exchanged during such events, under strong baroclinic forcing. The sum of V_u induced by all the upwelling events occurring on a given year N_u provides an estimate of the total volume exchanged between the lake and the embayment induced by strong baroclinic forcing during that year. In 1995 and 1999 that yearly estimate was, respectively, above and below the average of the 18-yr time series. Six releases were performed each year, 30 d apart and starting on day 90. The tracer content in LSB was tracked for 270 d in each experiment. Thereafter, the tail of the FTD was calculated assuming internal complete mixing (i.e., an exponential decay). The rate of decay for the tail is calculated by fitting an exponential model to the tracer mass within the embayment versus time curve for the last 120 d of the simulation.

Figure 12a shows the first moment of the FTD curves for each of the six simulations and for each of the 2 yr. During summer releases the determined mean flushing times are approximately 35–40% shorter than during the spring and fall

experiments, indicative of more active transport during the stratified season. More importantly, the mean flushing times in 1995 (with larger $N_u \times t_u \times \Delta T_c$) are between 25% and 40% shorter than in 1999, suggesting that a considerable part of the interannual variability in transport rates is due to changes in frequency and duration of upwelling events in LO. Figure 12b shows the FTD for a tracer released on day 150, 1995, which has been smoothed with a 7-d moving average filter. The peaks in the FTD indicate periods with active exchange, and they correspond to upwelling events (peaks in the reduced-gravity time series, Fig. 12c). The flushing time distribution curves, and hence the value of their moments, are shaped by the occurrence of episodic events of large baroclinic gradients across the lake–embayment connection.

Residence times.—In the construction of residence time curves, the alongshore currents in LO are presumed to be strong enough that all water leaving the channel is immediately carried away and replaced by lake water. By adopting this assumption, (1) one only needs to include LSB and the channel in the computational domain, simplifying the problem considerably and reducing the execution time; (2) the rate of mass loss versus time $r(t)$ in these calculations becomes a true representation of the RTD, $\varphi(t)$; (3) one does not represent the behavior of biogeochemical constituents that can return to LSB without being modified in LO; and (4) the barotropic processes become very efficient as exchange mechanisms (all mass leaving the channel during a seiche cycle is lost), in contrast with the case when part of the water exiting the embayment during ebb returns during flood (this case was considered in the analysis of flushing times).

Although it can be argued that this is a strong simplification of the nature of the exchange phenomena, the focus of the experiments in this section is to reveal (1) the magnitude of the spatial variability of residence times within the embayment, and (2) the effects of the relative position (in time) between upwelling events and release times on their mean residence time. In addition, the RTD calculated in these experiments is a true representation of the RTD of a biogeochemical component for which exposure to the lake environment implies instantaneous degradation or death. An individual or particle of this component would immediately disappear upon exiting LSB into LO.

A total of eight tracer experiments were simulated using data from year 1995 to drive the model. A fixed amount of tracer was released in LSB on days 90, 150, and every 20 d thereafter, at five different horizontal locations (Fig. 12c,d). At each horizontal location two tracer slugs were released: at the surface (1.5 m deep) and at the bottom of the water column. Hence, a total of 10 tracer slugs were released in every experiment, and they are identified with a number (1 to 5) according to their horizontal location and with a letter that indicates whether the release point is surficial (S) or deep (D). Each experiment lasts 270 d, and again in this case, the tail of the RTD is calculated presuming internal complete mixing after this 9-month period.

Figure 12d shows the first moment of the RTD for all the experiments and all tracers. At the beginning of the season

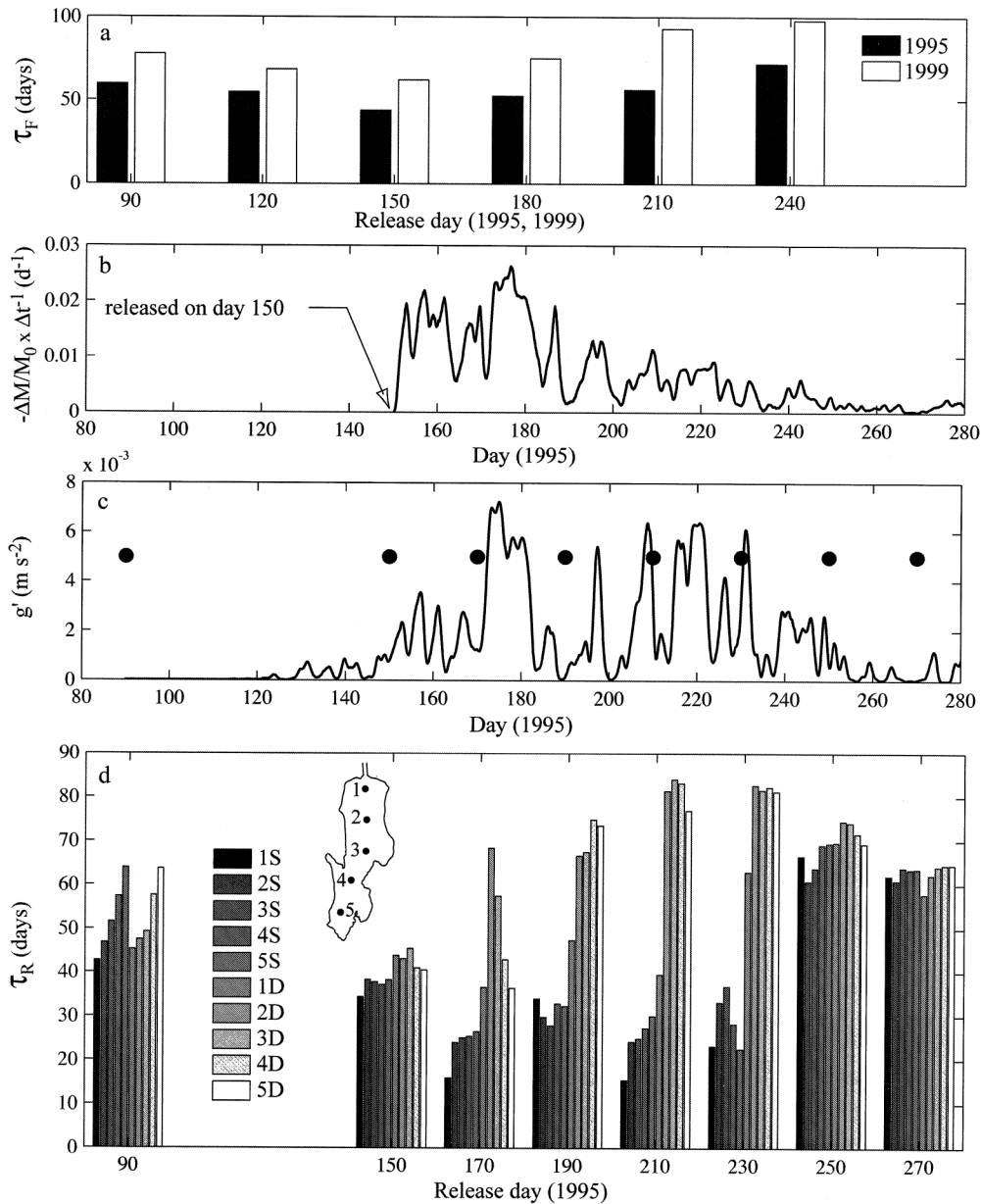


Fig. 12. Results of long-term experiments to determine transport timescales in LSB. (a) Mean flushing times τ_F for six tracer releases every 30 d starting on day 90, in two different years (1995 and 1999). (b) Flushing time distribution for a tracer released on day 150, 1995. (c) Time series of reduced gravity, g' , calculated from simulated surface and bottom temperatures at the center of the lake–bay connection. The peaks mark periods of strong lake–bay temperature differences. The black dots indicate the day of release for residence time numerical experiments in 1995. (d) Mean residence times, τ_R , for the experiments in 1995. The spatial location of the release in each experiment is identified with a number (its horizontal location—shown on the map) and a letter (its vertical location—S for surface and D for deep).

(day 90 release) the average mean residence time is about 50 d, and it is the horizontal location of the release that determines the differences in mean residence time. As the annual cycle progresses the spatial variation of mean residence time increases and it is principally explained by the vertical release location. Stratification inhibits the vertical motion of substances and accelerates horizontal transport in the surface layers. The mean residence time for the 10 trac-

ers released on day 190 is again 50 d, ranging from 30 d at the surface to 80 d at depth. At the end of the season, spatial gradients of the mean residence time vanish while the average mean residence time for all 10 releases is longer (60–65 d on average).

The seasonal changes in mean residence times can be better understood by considering the canonical form of a residence time distribution for a purely diffusive system. The

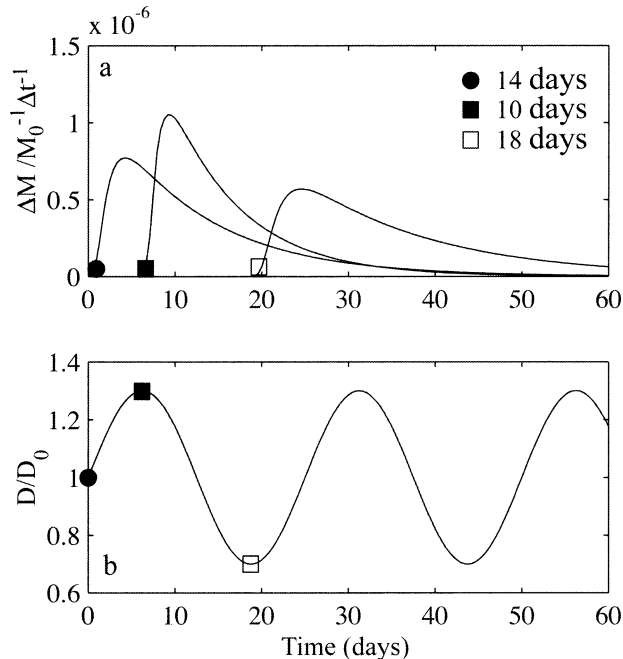


Fig. 13. Exchange processes in a 1-D diffusion model of transport, proposed by Dronkers and Zimmerman (1982) for a “tidal” subembayment with negligible through-flow on intertidal timescales. The diffusion equation for a tracer C is solved using a Crank–Nicholson scheme, subject to: (1) $C(x = L, t) = 0, t \geq 0$; (2) $dC/dt(x = 0, t) = 0, t \geq 0$; and (3) $C(x, 0) = \delta(L/8)$, where δ is the Dirac-delta function. (a) Residence time curves for a series of releases in a system with variable diffusion coefficient, D . Each curve is identified with a symbol. The diffusion coefficient is presumed constant in space and varies with time as shown in (b) around a mean value D_0 . The symbols in (b) mark the release times for each curve shown in (a). The mean residence times (in days) for the curves are shown for each release shown in the plot.

diffusive model has been proposed by Dronkers and Zimmerman (1982) to represent semienclosed tidal embayments at intertidal timescales. Figure 13 shows RTDs of such a system for a uniform diffusion coefficient, with an increase shortly after the release and a slow decay thereafter. This is also the shape of the RTD for LSB at monthly or bimonthly timescales. By using a diffusion coefficient D with a sinusoidal variation around an average value D_0 , one can mimic the seasonal effects of stratification. The characteristic timescales for the changes in the diffusion coefficients are chosen to be of the same order as the mean residence time for a system with $D = D_0$, as is the case of LSB. These simple experiments show that the value of the diffusion coefficient at the release time and shortly after is critical, as it determines changes in the shape of the RTD and hence its mean value. For $D > D_0$ shortly after the release, the RTD has a more pronounced increase and a faster decay, and the mean residence time decreases. For $D < D_0$, the RTD has a less pronounced increase, a slower decay, and its first moment increases. This effect appears in the RTD calculated with the 3-D model. The transport rates immediately after the fall releases (day 270), during the winter months, is low; the

initial increase in the RTD curve is reduced, and the fluxes as one moves away from the release time become larger.

At the seasonal timescale the transport rate at the time of release has a considerable effect on the mean residence time. On much shorter timescales (order several days to weeks), this sensitivity to exchange rates at release time also occurs. Two major upwelling events occur shortly after days 170 and 210, 1995 (see Fig. 12). In nonlinear systems these events have profound consequences that cannot be ignored or captured by simply assuming “average” physical conditions. The tracer slugs at 1S released on days 170 and 210 encounter a very active transport system (especially close to the connection) and hence the length of time that, on average, water at this location remains in the system is only 15 d. This is almost one-half the mean residence time determined at that same location 2 weeks before or after the major upwelling event, and 20–30% lower than the mean residence time away from the lake–embayment connection.

Observations and numerical simulations have been used in this work to study the transport timescales (residence and flushing times) in a small freshwater embayment (LSB) with negligible through-flow but permanent connection to a large lake (LO) through a shallow, narrow, and long channel. Given that the assumptions underlying simplistic approaches to calculating transport timescales do not apply to these systems, the residence and flushing timescales have been evaluated using tracer releases with a 3-D hydrodynamic model. The results of the simulations indicate that the mean residence time in LSB varies from 15 to 80 d and is subject to changes both in space and time. Its magnitude is of the same order as the timescale of seasonal changes in stratification, allowing complex patterns of intermittent exchange events to determine these timescales. Therefore, the analysis of residence times needs to be done across seasonal and interannual timescales. Transport, in weakly forced systems like LSB, is forced by variable and weak winds, oscillations in the water level—which, even in extreme cases, are at most on the order of several centimeters—and spatial thermal variations. Horizontal density-driven processes are shown here to be the dominant transport mechanism. Temperature gradients across the lake–embayment connection are the result of (1) differences in thermal inertia, at the seasonal timescales; and (2) at shorter timescales (of one to several days), differences in the internal dynamics of the two water bodies connected through the channel. As shown by Rueda and Cowen (2005), the largest density gradients along the channel are caused by episodic upwelling events in LO during the stratified season, driven by easterly and southeasterly wind events. In theory, wind could also upwell cold hypolimnetic water in the northern end of the embayment, inducing large temperature gradients along the LSB–LO connection. The strong wind events around day 217, 2002 shows, partially, that this is in fact the case. The exchange rates during upwelling events are shown here to be an order of magnitude larger than the exchange rates associated with barotropic processes (changes in lake levels), and thermal inertia-driven baroclinic processes. These results indicate that the renewal rates in freshwater embayments like LSB depend on the occurrence of upwelling events, the thermal

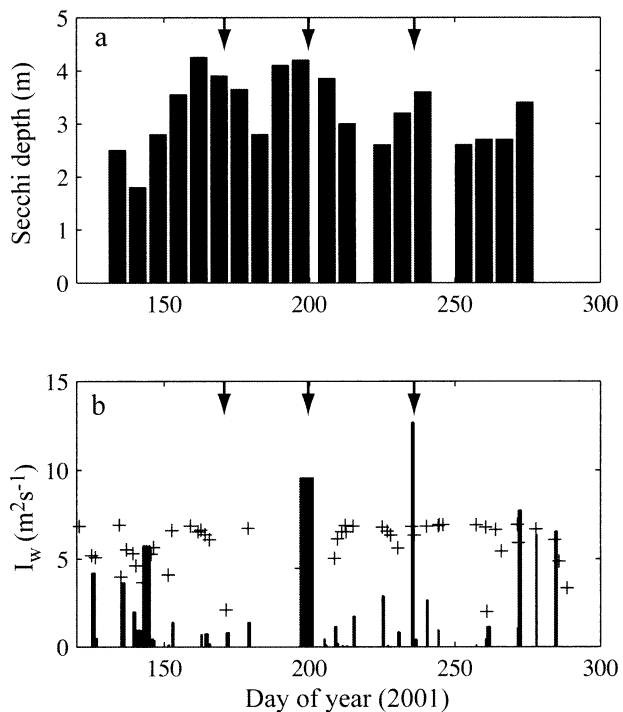


Fig. 14. (a) Secchi depth observations (Doyle and Hairston pers. comm.) for LSB in 2001. (b) Series of alongshore impulses of upwelling-favorable wind events (bars), and threshold values for the alongshore wind impulse to induce a full upwelling event (crosses). Calculations are on the basis of wind records from buoys 45139 and 45135 (operated by Environment Canada) in the northern and western ends of LO, respectively. The arrows in (a) and (b) mark periods when the wind records suggest that upwelling events could have occurred.

gradients induced across the connections, and their duration and frequency.

The long-term simulations suggest that interannual variations in the magnitude of the transport timescales in LSB are related to year-to-year changes in the number of upwelling events in LO: the larger the number of upwelling events in LO, the smaller the simulated mean flushing times in LSB. The control by upwelling frequency of the transport rates has strong implications for the study of spatial patterns of transport in embayments along LO's shoreline. Given that the winds in the lake are predominantly from the west (Phillips and Almazan 1981), one would expect faster renewal rates in embayments located along the west and north shores relative to embayments along the lake's southern and eastern shores. Upwelling frequency also has implications on the spatiotemporal patterns of primary productivity in freshwater embayments that, like LSB, have small watersheds and hence weak nutrient fluxes from the tributary inflows. Large fluxes of nutrient-rich hypolimnetic lake water entering the embayment during upwelling events could potentially induce increased rates of net phytoplankton production, and hence influence the population dynamics within the ecosystem. Figure 14, which shows Secchi disk depth measurements (a simple and quick measure of primary productivity) taken in LSB during 2001 (Doyle and Hairston pers. comm.) together

with time series of easterly wind impulse, I_w (the integral over time of the wind stress during an individual event), in LO, is very suggestive in this regard. Upwelling events occur if the alongshore easterly wind impulse is larger than a threshold value, determined by stratification conditions in the water column and the magnitude of offshore (southerly) winds. Thermal stratification in LO is presumed constant, characterized by a 14-m-deep thermocline and a reduced gravity of ca. $1.5 \times 10^{-3} \text{ m s}^{-2}$, typical of summer conditions (Schwab 1977). The Secchi depth time series shows cyclic changes, which are typical of lake environments (see for example fig. 7 in Thomann et al. 1981). Each of the three upwelling events that occurred in the three summer months of 2001 precede periods of decreases in water transparency, as indicated by negative trends in the Secchi depths. We hypothesize that these decreases in transparency are the result of increased biological activity. While suggestive, it remains to be proven whether fluctuations in biological activity reflect an endogenous response of the system or are driven by exogenous (upwelling) influences.

This research has focused on understanding water movement in a freshwater embayment, without considering the "environmental conditions" (pH, light, dissolved oxygen) that any given water parcel encounters on its trajectory as it leaves the system. The impact of varying these conditions could be of extraordinary importance to determining the outcome (fate) of a reactive transport process. A Lagrangian approach to water quality, which incorporates "along the path" variations, will be required to understand in detail the true role of water residence times in determining or influencing the biogeochemical behavior of any aquatic system. Water residence time, per se, is likely to be the determining factor for reactive transport if the system has homogenous environmental conditions, which is not the case in a natural freshwater system, even one with small dimensions. If water residence times are not the key parameters in the characterization of natural reactors, a question that future research will need to address is whether there exists a unique timescale that characterizes the ecosystem considered as an entity.

References

- ANDRADOTTIR, H. O., AND H. M. NEPF. 2001. Impact of exchange flows on wetland flushing. *Water Resour. Res.* **37**: 3265–3273.
- ARMI, L., AND D. M. FARMER. 1986. Maximal two-layer exchange through a contraction with barotropic net flow. *J. Fluid Mech.* **164**: 27–51.
- BECKMANN, A., AND R. DOSCHER. 1997. A method for improved representation of dense water spreading over topography in geopotential-coordinate models. *J. Phys. Oceanogr.* **27**: 581–591.
- CLARK, M. M. 1996. Transport modeling for environmental engineers and scientists. Wiley-Interscience.
- DEE, D. P. 1995. A pragmatic approach to model validation, p. 1–13. *In* D. R. Lynch and A. M. Davies [eds.], Quantitative skill assessment of coastal ocean models. American Geophysical Union.
- DEGAETANO, A. T., K. L. EGGLESTON, AND W. W. KNAPP. 1993. Daily Solar Radiation Estimates for the Northeastern United States. Research Publication RR 93-4, Northeast Regional Climate Center.

- , ———, AND ———. 1994. A comparison of solar radiation estimates for the Northeastern United States using the Northeast Regional Climate Center and National Renewable Energy Laboratory models. *Solar Energy* **55**: 185–194.
- DRONKERS, J., AND J. T. F. ZIMMERMAN. 1982. Some principles of mixing in tidal lagoons. *Oceanol. Acta (suppl.)* **4**: 107–118.
- FAIRALL, C. W., E. F. BRADLEY, D. P. ROGERS, J. EDSON, AND G. YOUNG. 1996. Bulk parameterization of air-sea fluxes for Tropical Ocean-Global Atmosphere Response Experiment. *J. Geophys. Res.* **101**: 3747–3764.
- FARMER, D. M., AND L. ARMI. 1986. Maximal two-layer exchange over a sill and through the combination of a sill and a contraction with barotropic flow. *J. Fluid Mech.* **164**: 53–76.
- FISCHER, H. B., E. J. LIST, R. C. Y. KOH, J. IMBERGER, AND N. H. BROOKS. 1979. Mixing in inland and coastal waters. Academic.
- FUSSMAN, G. F., S. P. ELLNER, K. W. SHERTZER, AND N. G. HAIRSTON. 2000. Crossing the Hopf bifurcation in a live predator-prey system. *Science* **290**: 1358–1360.
- GRIFFIES, S. M., AND R. W. HALLBERG. 2000. Biharmonic friction with a Smagorinsky-like viscosity for use in large-scale eddy-permitting ocean models. *Month. Weather Rev.* **128**: 2935–2946.
- GROSS, E. S., V. CASULLI, L. BONAVENTURA, AND J. R. KOSEFF. 1998. A semi-implicit method for vertical transport in multi-dimensional models. *Int. J. Num. Methods Fluids* **28**: 157–186.
- HILTON, A. B. C., D. L. MCGILLIVARY, AND E. E. ADAMS. 1998. Residence time of freshwater in Boston's inner harbor. *J. Water. Port Coast. Ocean Eng.* **124**: 82–89.
- HODGES, B. R., J. IMBERGER, A. SAGGIO, AND K. B. WINTERS. 2000. Modeling basin-scale motions in a stratified lake. *Limnol. Oceanogr.* **45**: 1603–1620.
- HOGG, A. M., G. N. IVEY, AND K. B. WINTERS. 2001. Hydraulics and mixing in controlled exchange flows. *J. Geophys. Res.* **106**: 959–972.
- IVEY, G. N. 2004. Stratification and mixing in sea straits. *Deep Sea Res. II* **51**: 441–453.
- JIN, K.-R., J. H. HAMRICK, AND T. TISDALE. 2000. Application of three-dimensional hydrodynamic model for Lake Okeechobee. *J. Hydraul. Eng.* **126**: 758–771.
- KANTHA, L. H., AND C. A. CLAYSON. 1994. An improved mixed layer model for geophysical applications. *J. Geophys. Res.* **99**: 25235–25266.
- LEVENSPIEL, O. 1999. *Chemical reaction engineering*. Wiley.
- MARTIN, J. L., AND S. C. MCCUTCHEON. 1999. *Hydrodynamics and transport for water quality modeling*. Lewis.
- MONSEN, N. E., J. E. CLOERN, L. V. LUCAS, AND S. G. MONISMITH. 2002. A comment on the use of flushing time, residence time, and age as transport time scales. *Limnol. Oceanogr.* **47**: 1545–1553.
- OFFICER, C. B. 1976. *Physical oceanography of estuaries*. Wiley.
- PHILLIPS, D. W., AND J. A. ALMAZAN. 1981. Meteorological analysis, p. 17–50. *In* E. J. Aubert and T. L. Richards [eds.], IFGL—the international field year for the Great Lakes. NOAA.
- ROSE, W. J., D. M. ROBERTSON, AND E. A. MERGENER. 2004. *Water quality, hydrology, and the effects of changes in phosphorus loading to Pike Lake, Washington County, Wisconsin, with special emphasis on inlet-to-outlet short-circuiting*. USGS-Scientific Investigations Report 2004-5141.
- RUEDA, F. J. 2001. *A three-dimensional hydrodynamic and transport model for lake environments*. Ph.D. dissertation, Univ. of California, Davis.
- , AND E. A. COWEN. 2005. Exchange between a freshwater embayment and a large lake through a long shallow channel. *Limnol. Oceanogr.* **50**: 169–183.
- , AND S. G. SCHLADOW. 2002. Quantitative comparison of models for barotropic response of homogeneous basins. *J. Hydraul. Eng.* **128**: 201–213.
- , AND ———. 2003. The internal dynamics of a large polymictic lake. Part II: Three-dimensional numerical simulations. *J. Hydraul. Eng.* **129**: 92–101.
- , ———, AND S. O. PALMARSSON. 2003. Basin-scale internal wave dynamics during a winter cooling period in a large lake. *J. Geophys. Res.* **108**: art. no. 3097.
- SANFORD, L. P., W. C. BOICOURT, AND S. R. RIVES. 1992. Model for estimating tidal flushing of small embayments. *J. Water. Port, Coast. Ocean Eng.* **118**: 635–654.
- SCHWAB, D. J. 1977. *Internal free oscillations in Lake Ontario*. *Limnol. Oceanogr.* **22**: 700–708.
- SMITH, P. E. 1997. *A three-dimensional, finite-difference model for estuarine circulation*. Ph.D. dissertation, Univ. of California, Davis.
- STOMMEL, H., AND H. G. FARMER. 1952. On the nature of estuarine circulation. Reference nos. 52–51, 52–63, 52–88 (3 vols. containing chapters 1–4 and 7), Woods Hole Oceanographic Institute.
- THOMANN, R. V., D. M. D. TORO, D. SCAVIA, AND A. ROBERTSON. 1981. Ecosystem and water quality modeling, p. 353–366. *In* E. J. Aubert and T. L. Richards [eds.], IFYGL—the international year for the Great Lakes. NOAA.
- ZIMMERMAN, J. T. F. 1976. Mixing and flushing of tidal embayments in the western Dutch Wadden Sea. Part I: Distribution of salinity and calculation of mixing time scales. *Neth. J. Sea Res.* **10**: 149–191.

Received: 19 October 2004

Accepted: 17 March 2005

Amended: 20 May 2005